Multidisciplinary | Rapid Review | Open Access Journal

Received October 25, 2020, accepted November 3, 2020, date of publication November 11, 2020,
date of current version November 25, 2020.

Digital Object Identifier 10.1109/ACCESS.2020.3037190

Additive Manufacturing and Testing of a Soft Magnetic Rotor for a Switched Reluctance Motor

LEONIDAS GARGALIS[1], VINCENZO MADONNA[2], (Member, IEEE), PAOLO GIANGRANDE[2], (Senior Member, IEEE), ROBERTO ROCCA[3], (Member, IEEE), MARK HARDY[1], IAN ASHCROFT[1], MICHAEL GALEA[2,4], (Senior Member, IEEE), AND RICHARD HAGUE[1]

[1]Centre for Additive Manufacturing (CfAM), Faculty of Engineering, University of Nottingham, Nottingham NG7 2GW, U.K.
[2]Power Electronics, Machines and Control Group, Faculty of Engineering, University of Nottingham, Nottingham NG7 2RD, U.K.
[3]Research Centre for Energy Resources and Consumption (CIRCE), 50018 Zaragoza, Spain
[4]Key Laboratory of More Electric Aircraft Technology of Zhejiang Province, University of Nottingham Ningbo, Ningbo 315100, China

Corresponding author: Leonidas Gargalis (Leonidas.gargalis@nottingham.ac.uk)

This work was supported in part by the Clean Sky 2 Joint Undertaking through the European Union's Horizon 2020 Research and Innovation Programme under Grant 807081, in part by the University of Nottingham Centre for Additive Manufacturing and Propulsion Futures Beacon, and in part by the INNOVATIVE Doctoral Programme, funded by the Marie Curie Initial Training Networks (ITN) Action under Project 665468.

ABSTRACT Additive manufacturing is acknowledged as a key enabling technology, although its adoption is still constrained to niche applications. A promising area for this technology is the production of electrical machines (EMs) and/or their main components (e.g. magnetic cores, windings, heat exchangers, etc.) due to the potential of creating lightweight, highly efficient rotating motors, suitable for applications requiring a low moment of inertia. This work investigates the readiness of metal additive manufacturing, specifically Laser Powder Bed Fusion (LPBF), applied to the field of EMs to bridge the gaps of how to use this technological approach in this field. A soft magnetic material featuring high silicon content (Fe-5.0%w.t.Si) has been developed for LPBF and a rotor has been 3D-printed for a switched reluctance machine. The printed rotor was assembled into a conventionally laminated stator and the performance of the whole machine was evaluated. Its performance was compared against an identical machine equipped with a laminated rotor of the same dimensions made of conventional non-oriented silicon steel. A comparative study was carried out through both finite element simulations and experimental tests. The efficiency of the two machines was assessed together with the principal electrical and mechanical quantities under several operating conditions.

INDEX TERMS Additive manufacturing, laser powder bed fusion, soft magnetic material, silicon steel, switched reluctance machine, 3D printed rotor, finite element simulation, AC electric drives.

I. INTRODUCTION

In conventional manufacturing methodologies, a component is built through a process of material removal, based on engineering drawing or sketches, such as milling. This approach is in contrast to that adopted by additive manufacturing (AM) technologies, where manufacturing data is generated by a computer aided design (CAD) and model process-specific software to accurately create complex geometric shapes via layer-by-layer material deposition and consolidation [1].

The associate editor coordinating the review of this manuscript and approving it for publication was Ahmed A. Zaki Diab.

Despite the various challenges [2], AM is perceived as an enabling technology, because it allows the development of parts and components with unprecedented freedom in geometry at little extra cost by minimizing the amount of wasted material (i.e. smart material utilization) [3]. AM technologies have only recently been utilised in the development of parts for electrical machines (EMs) [4]–[6], which can be attributed to the lack of AM processable materials with the necessary properties for such applications [7].

Among AM build strategies, the laser powder bed fusion (LPBF) method is the most suitable for producing highly detailed metallic parts [3] and it has been

extensively applied in manufacturing structural materials. Indeed, near net-shape components are manufactured by selectively melting metallic powder, layer upon layer, through a high-intensity laser [1]. After cooling, a solid metal, near fully dense (ref) part is consequently created and the extremely rapid melting/cooling process leads to a fine grain microstructure [9]. Only recently, LPBF has found application in the processing of electrically conductive [10], [11] and soft magnetic materials [12]–[17] potentially enabling the demand for high performance lightweight EMs.

In literature, several examples of EM components fabricated via LPBF process can be found, although comprehensive analyses, accounting for the experimental comparison between 3D printed and conventionally manufactured EMs, are difficult to find. The viability of the LPBF technology is demonstrated in [5], which features the rotor structure of a synchronous reluctance machine. Details regarding the feedstock metallic powder are given along with the magnetization curve (i.e. MH curve) of the soft magnetic material, but measured performance of the synchronous reluctance machine is not included. The design of an AM synchronous reluctance machine is introduced in [18] and the ensuing benefits against the traditional design are quantified via finite element (FE) simulations at rated speed confirming the 1% efficiency increment. In [6], a permanent magnet synchronous machine is demonstrated, whose 3D printed rotor features enhanced magnetic anisotropy to improve the sensorless control capability of the machine. The trend of the magnetic anisotropy as function of the injected signal frequency is provided. A weight reduction of about 25% compared to the conventional design is achieved in [19], where a new soft magnetic material is employed in the rotor shaft of a permanent magnet synchronous EM. The lightweight shaft led to lower moment of inertia, resulting in shorter acceleration time.

All the above deal with various aspects of AM for EMs, however, they all stop short when it comes to a complete process of how AM fares for the production of EMs. There is still a missing completeness that will enable the community of EMs to fully capitalise on the AM capability and potential. Thus, in this work, a complete study focusing on AM technology implementation for an EM component is presented, with the purpose of evaluating and assessing the system-level performance (i.e. output torque and efficiency) of the switched reluctance machine (SRM) mounted with a 3D printed rotor. A commercially available SRM is selected as a benchmark EM, whose rotor is characterized by a laminated structure of non-oriented silicon steel. The SRM is the motor type that suits best the goals of AM electric motor manufacturing as they lack permanent magnets, they have concentrated windings and the rotor can be optimized with the use of computational design for AM [20]. A metallic powder with high silicon content (Fe-5.0%w.t. Si) is synthesized and preliminary tests are carried out on different samples to identify its principal physical properties (i.e. magnetization curve, tensile stress, mass density, etc.). After testing the magnetic and mechanical properties of the 3D printed soft magnetic material, 2D FE simulations are used, aiming to outline the SRM performance with a rotor core made of the high silicon content material. The soft magnetic material is then processed via LPBF to produce a solid piece rotor mirroring the exact geometry of the benchmark one. The 3D printed rotor is finally integrated into the stator of the laminated benchmark rotor. The results collected on the SRM equipped with the 3D printed rotor are then compared to those related to the benchmark SRM.

TABLE 1. Parameters of the Benchmark SRM.

Parameter	Value
Rated Speed	600 rpm
Rated Torque	17.2 Nm
Rated Voltage	360 V_{pk}
Number of Slot	12
Number of Pole	8
Axial Length	104 mm
Stator Outer Diameter	150 mm
Rotor Outer Diameter	79.2 mm
Number of Turns	220x4

II. BENCHMARK SRM

The SRM is a singly excited, doubly salient EM, where the energy conversion occurs in discrete cycles exploiting the tendency of the rotor to align spontaneously with the stator according to the principle of minimum magnetic reluctance path [21]. In recent years, SRMs have gained renewed attention in both the academic and the industrial world, because of their rugged and robust structure, as well as independence from permanent magnets [22], [23]. SRMs are suitable for a wide range of constant power speeds and can operate in harsh environments [21]. Although SRM control relies on more advanced and complex strategies than most alternatives, the mentioned benefits led the SRM to being considered a substitute to permanent magnet and induction machines in many applications such as aerospace, automotive, industrial and energy storage.

In this work, an off-the-shelf, three-phase SRM was chosen as the benchmark EM. The selected SRM has 12 slots and 8 poles and its rated values are listed in Table 1 along with the main geometrical dimensions. In particular, the outer diameter of stator and rotor and the axial length were 150 mm, 79.2 mm and 104 mm, respectively.

Both stator and rotor cores comprise laminated structures featuring 0.35 mm thick sheets made of non-oriented silicon steel M800 (Fe-3.5%w.t. Si).

The cross-sectional view of the machine and its winding layout are shown in Fig. 1. Each phase has a total of 4 series-connected coils with 220 turns each. The measured DC phase resistance at 20 °C was 10Ω.

A standard, commercial converter implementing a soft-switching strategy was used to control the machine. The controller receives the rotor position feedback from a simple

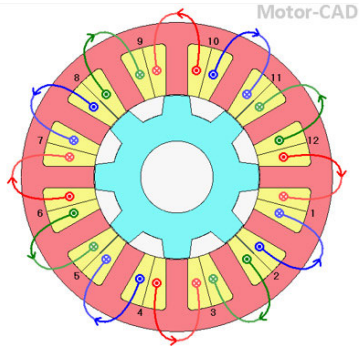

FIGURE 1. Cross-sectional view and winding layout of the case study SRM.

optical position sensor using three photodiodes and three light emitting devices. Based on the rotor position, the control algorithm generated and sent the control signals to the switching devices. A digital hysteresis control algorithm was used to maintain a flat-topped current when the SRM operated at low speed (i.e. the phase voltage was chopped to maintain the current within the hysteresis band). The turn-on and turn-off angles of each phase were automatically selected, according to the instantaneous torque request to minimized the required current (i.e. maximum torque per ampere algorithm).

III. SOFT MAGNETIC MATERIAK WITH HIGH SILICON CONTENT AND ROTOR 3D PRINTING

For manufacturing the stator and rotor cores, the most popular materials are electrical steels, which can be classified in two categories, namely silicon-based steels (Fe-Si) [24] and cobalt-based steels (Fe-Co) [25]. The former represents a common choice, as with the benchmark SRM, due to lower cost, while the latter is preferred in high performance EMs. Silicon-based steels are alloys with silicon content between 1% and 6.5% w.t. The addition of silicon increases the electrical resistivity of steel and, therefore, reduces eddy current losses. However, with increasing silicon content, the material becomes harder and more brittle, and thus more difficult to process [26], [27].

A. POWDER BLEND AND SAMPLES PREPARATION

In this study a silicon steel powder blend with Fe-5.0%w.t. Si was produced, by mixing a high silicon steel pre-alloyed (Fe-6.9%w.t.Si) with high purity Fe powder (99.9%w.t.Fe). The scanning electron microscope (SEM) micrographs of both parent powders and resulting powder blend are shown in Fig 2. The particle size for the pre-alloyed Fe-Si powder ranged between 20 μm and 60 μm diameter, while that of pure iron had an average diameter of 10 μm. Therefore, the powder blend shown in Fig. 2c resulted in an average particle diameter of 36.2 μm, thus enabling efficient spreading and high packing density on the powder bed.

The powder blend was dried at 70 °C for 2 hours before the LPBF process, which was carried out using a Renishaw AM125 LPBF machine equipped with a 200 W D-series redPOWER ytterbium fibre continuous wavelength laser. The

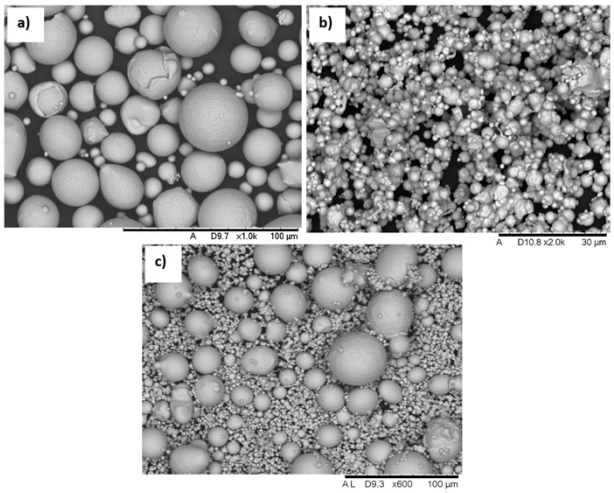

FIGURE 2. SEM micrographs of metallic powders a) pre-alloyed Fe-6.9%w.t. Si, b) pure iron Fe (99.9%) and c) Fe-5.0%w.t. Si powder blend.

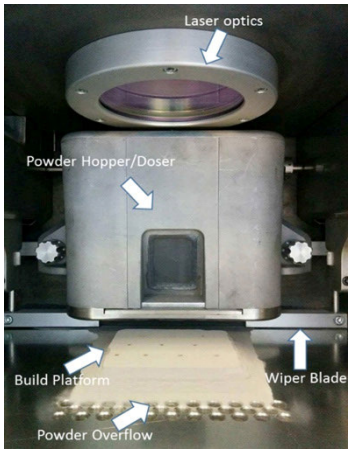

FIGURE 3. Build chamber configuration.

laser spot size was 35 μm ($\pm 5\mu$m) with a laser power density of 20.8 MW/cm^2. The LPBF process was conducted under argon atmosphere with an oxygen level below 500 ppm to reduce oxidation. The preliminary samples were built on mild steel substrates that were pre-heated to 170 °C. This temperature was kept constant throughout the manufacturing process to reduce thermal gradients and hence residual stress. The configuration of the build chamber is illustrated in Fig. 3, whilst the optimal parameters for maximum density are reported in Table 2.

According to the setting of Table 2, samples with different shapes (i.e. cube shape, cylindrical dog-bone shape, etc.) were produced to determine the physical, magnetic and mechanical properties of the developed high silicon content material, as depicted in Fig. 4.

B. PHYSICAL PROPERTIES OF FE-5WT% SI PROCESSED BY LPBF

Standard 5mm cubic samples were used to analyse 3D printed material density as shown in Fig. 4a). Once printed, these samples were cross-sectioned and encapsulated in a

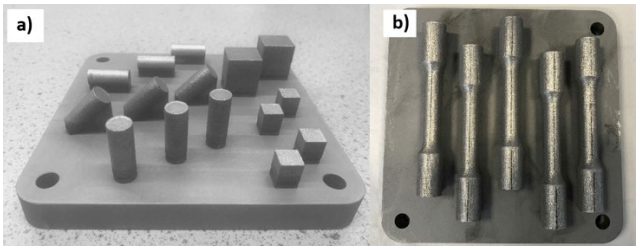

FIGURE 4. Samples for the characterization of a) density and magneic properties and b) mechanical properties.

TABLE 2. LPBF process parameters setting.

Parameter	Value
Maximum Laser Power	200 W
Minimum Laser Spot Diameter	35 µm
Powder Bed Temperature	170°C
Laser Scan Speed	800 mm/s
Layer Thickness	30 µm
Laser Beam Focus Position	0 mm
Hatch Spacing	110 µm
Scan Strategy	Meander 67° rotation/layer

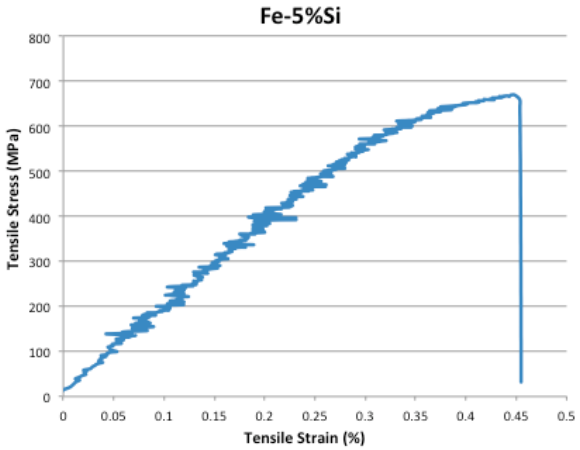

FIGURE 5. Tensile stress–strain curve of additively manufactured Fe-5%w.t. Si sample.

pressurised hot mount resin. They were then grounded flat and polished to acquire optical micrographs. The optical density measurements were carried out through the open source software ImageJ Fiji [28] and the achievement of a near fully dense structure (i.e. 99.9%) was confirmed.

Cylindrical dog-bones compliant to ASTM standard E8/E8M [29] were 3D printed (Fig. 4b)) and machined to perform the tensile tests. A representative tensile test result is shown in Figure 5. The resulting mechanical properties of the as-built parts are well above the required/minimum yield strength of 400MPa of conventional lamination steels with 3.5%w.t. silicon content. The Fe-5%w.t.Si processed with LPBF, features near zero ductility. Moreover, its hardness of

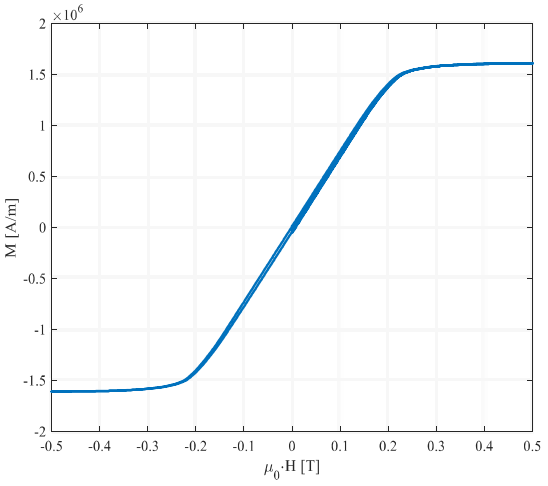

FIGURE 6. Magnetisation (BM) curve of additively manufactured Fe-5%w.t.Si sample.

270HV, (Vickers Hardness) [30], makes it a difficult material to process with traditional manufacturing methods.

A final set of cylindrical samples was machined so that the diameter was 4mm and the mass of each sample did not exceed 1g resulting in a total saturation magnetisation up to 300emu. A vibrating sample magnetometer was used for the characterisation of magnetic properties. In Figure 6 the magnetization curve (i.e. BM curve) is illustrated and on average the 3D printed material was characterised by a maximum relative permeability of about 2200, a saturation magnetisation of 1.22 T, a residual magnetisation of 0.44 T and a coercivity of 80 A/m.

After characterising the magnetic properties of the developed high silicon content material (Fe-5.0%w.t. Si), the electromagnetic FE analysis on both SRMs was carried out (i.e. benchmark SRM mounting a laminated rotor and SRM equipped with an additively manufactured rotor), as examined in Section IV.

The average mass density value of the 3D printed material, was determined with the use of a Helium Pycnometer made by Micromeritics (USA), model AccuPyc 1330. Three samples with the same volume ($1cm^3$) as the reference sample of the pycnometer were printed. The mass density was $7.36g/cm^3$ averaged from 30 measurements in total (10 per sample). Rectangular test bars were printed in order to measure the electrical resistivity value of the 3D printed material in accordance to ASTM B193-02 "Standard Test Method for Resistivity of Electrical Conductor Materials" [31]. Electrical DC resistance testing was performed using a Valhalla Scientific Inc. (USA) 4300B digital micro-ohmmeter. This DC four-wire Kelvin resistance measurement meter was calibrated to within 5% accuracy. It was capable of generating a current between 0.1 mA and 10A and able to measure a voltage from 20 mV to 2V, with a minimum sensitivity of $1\mu V$. Specimens were individually measured along all dimensions, in a minimum of four places using Mitutoyo digital calipers, which had an accuracy of ± 0.02 mm. This

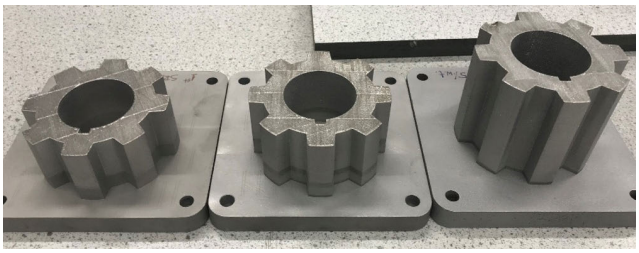

FIGURE 7. 3D printed segments on 125 × 125mm mild steel substrates, constituting the AM rotor.

was undertaken to accurately determine the cross-sectional area and length of each specimen. Electrical resistivity (ρ) measured in $\mu\Omega$-cm was calculated by $\rho = \text{RA/L}$, where R was the measured resistance in $\mu\Omega$, A was the measured external cross-sectional area of the specimen measured in cm^2, and L was the length of the specimen in cm. The average resistivity of the Fe-5%w.t.Si specimens was 104 $\mu\Omega$-cm.

C. 3D PRINTING OF THE SRM ROTOR

In the presented work, a step-by-step approach was applied to evaluate the viability of the AM technologies applied to various different components in EMs. For this reason, it was decided to 3D print only one out of the two SRM's ferromagnetic cores, namely the rotor core for the first case study. Indeed, the extra core losses arising from the choice of also having an AM stator might be a source of concern in terms of thermal management, due to the undersize of the benchmark SRM's cooling system. Therefore, the sole 8 poles rotor was additively manufactured and its dimensions mirrored those of the benchmark SRM's rotor. It should also be noted here, that the LPBF process potentially offers the scope for more efficient design through design routes such as topology optimisation [20] but in this case we keep the design and dimensions the same as the reference motor to concentrate this study on material performance. Due to build height restrictions in the LPBF machine, the 3D printed rotor made of Fe-5.0%w.t. Si was fabricated in three segments for an overall axial length of 104 mm, as depicted in Figure 7. Due to technical constraints with the LPBF system used, the rotor height was prohibitive for one build. Therefore the rotor was divided into three segments. In particular, the first segment featured an axial length of 54 mm, while the other two were 25 mm long. The final 3D printed rotor was composed of the three segments, and the ensuing eddy current paths along the axial direction were thus shorter compared to a single piece solution. Therefore, a positive impact on the containment of the eddy current losses was expected on the 3D printed rotor.

The samples were heat treated at 1150 °C for 1 hour to remove residual stress and improve the magnetic properties before removal from the substrate with the use of Electrical Discharge Machining (EDM). Next the samples were post build machined, to ensure the right tolerances and the three segments were assembled as a single piece on a mild steel key-locked shaft, with the same dimensions as the benchmark machine. The 3D printed rotor was mechanically balanced up to a speed of 3500 rpm, by removing the exceeding material from the mild steel lock rings. In Figure 8, the fully assembled 3D printed rotor is shown and compared to the laminated rotor of the benchmark SRM. In turn, both rotors of Figure 8 have been integrated into the benchmark SRM's stator and tested, as discussed in Section V. Knowing the magnetic properties of the high silicon content material (Fe-5%w.t.Si), a comparative analysis was performed on both SRMs through FE simulations, before moving to the experimental tests campaign.

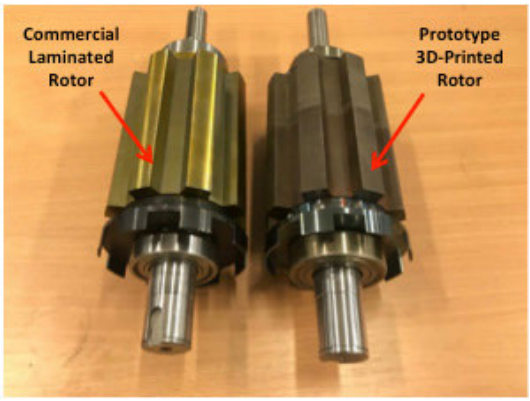

FIGURE 8. Commercial laminated 8-pole SRM rotor (left-hand side) and identical 3D printed rotor (right-hand side).

IV. SRMS FE ANALYSIS

Simulation of the predicted electromagnetic effect of using the 3DP-SRM was undertaken by 2D FE modelling. The FE simulations were carried out with the use of MotorCad, a proprietary Multiphysics software, sourced from Motor Design Ltd., UK. Two cases were investigated: 1) both stator and rotor ferromagnetic cores are made of M800 laminated silicon steel (i.e. benchmark SRM) and 2) the stator core material remained unchanged, while the rotor core, adopted the 3-piece high silicon content material (i.e. 3DP-SRM). The machine performance was evaluated in terms of generated electromagnetic torque, magnetic saturation level and losses. By determining the iron loss distribution we can calculate the iron losses of the rotor so that experimental results can be better analysed. In order to quantify the rotor loss variation, equation (1) was used, where P_{rot} were the rotor losses, P_{el} was the electrical input power, P_{Joule} were the winding Joule losses, P_{stat} were the stator iron losses, T was the shaft torque and ω_m was the mechanical speed. Windage losses are not included due to the relatively low operational speed.

$$P_{rot} \approx P_{el} - P_{Joule} - P_{stat} - T \cdot \omega_m \quad (1)$$

Figure 9 which is above, shows the flux map and magnetic field lines of the benchmark and 3DP-SRM while operating at base speed and delivering the rated (average) torque of 18.7 Nm. From this plot it was possible to verify that the magnetic core of the 3DP-SRM was slightly

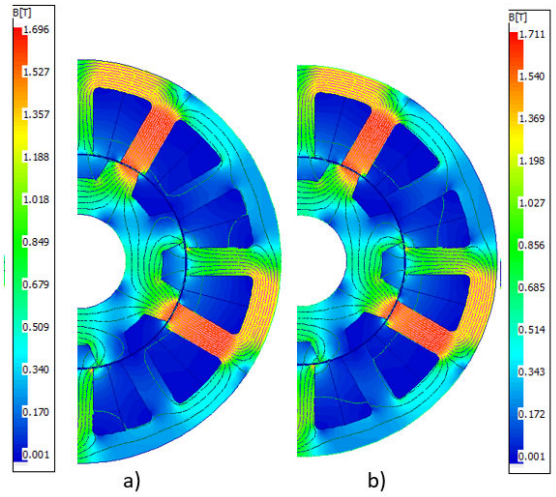

FIGURE 9. Flux density and magnetic field lines at rated operating condition for a) benchmark SRM and b) 3D printed SRM.

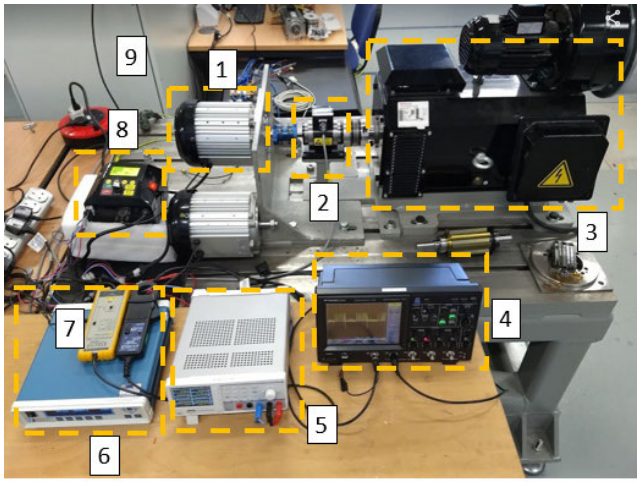

FIGURE 10. Experimental test-bed (analytical description provided in Table 3).

more saturated compared to the benchmark machine. Such an effect was more accentuated within the stator poles, meaning that the 3DP-SRM must be fed with a larger current (and ensuing larger magnetic flux density) to develop the rated torque. Moreover, a speed-sweep analysis was carried out to determine if there was any particular operating speed range in which the SRM developed excessive torque ripple. As a result it was found that within the range 800 – 1200 rpm an anomalous ripple could be observed. Therefore, experimental tests with the machine operating within the aforementioned speed range were avoided.

V. SRMS EXPERIMENTAL TESTS

This Section describes the experimental test procedure and reports the main results for both the benchmark and the 3DP-SRM.

TABLE 3. Test-bed Components / Instruments.

ID See Fig. 2V	Description
1	3DP-SRM
2	Magtrol torque-meter
3	Oswald induction machine (load)
4	Lecroy Wavetouch® oscilloscope
5	Rode & Shwarz power analyzer
6	Magtrol torque / speed data-logger
7	Pico current and voltage probes
8	Benchmark/Laminated SRM drive (converter)
9	Induction machine drive cabinet

A. TEST-BED DESCRIPTION

In order to test the electromechanical performances of the manufactured 3DP-SRM and to compare this with the benchmark machine, the test-bed shown in Figure 10 was used. The description of each component/instrument is reported in Table 3.

As shown in Figure 10, the SRM was flange-mounted to an "L" plate. Its shaft was mechanically coupled through a Magtrol® torque-meter to a 70 kW, variable-speed Oswald® induction motor. The load induction machine was torque controlled via an Emerson Unidrive® three-phase inverter.

Phase current and voltage were measured through a hall-effect current clamp and a differential probe respectively. These were connected to a Lecroy® Wavetouch oscilloscope for instantaneous time-domain analysis and logging. In addition, an instantaneous electric power analysis was carried out using a Rode & Shwarz power analyser, which records and processes the phase and current voltage.

B. TESTS RESULTS

Both machines (i.e. benchmark SRM and one with 3DP-SRM) were tested at various operating conditions, with the purpose of covering the entire torque / speed envelope. In particular, both machines were tested at more than 50 different operating points. For the sake of brevity the measured torque speed envelope, and efficiency maps are summarized in Figure 11 and 12 for the benchmark and 3D printed machines respectively.

At the rated speed (i.e. 600 rpm), the 3DP-SRM produced 13% less torque compared to the benchmark SRM. This was more clearly identifiable from the data reported in Table 4, where the measured electrical and mechanical quantities at rated speed are tabulated.

When the operating speed was increased, the performance of the 3DP-SRM tended to improve, both in terms of both maximum mechanical power and efficiency, as observed in Table 5, where the electric and mechanical power quantities, measured at 1500 rpm and maximum torque, are listed.

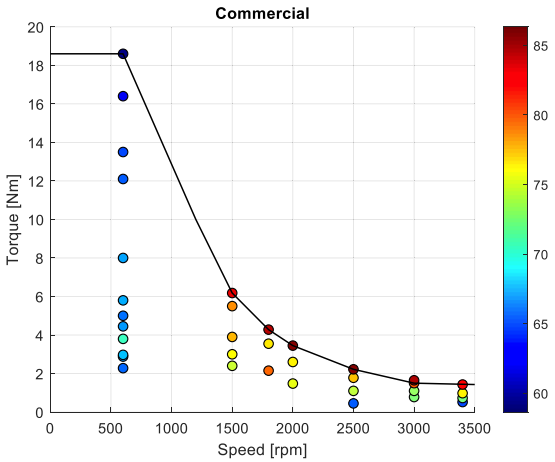

FIGURE 11. Measured efficiency map and torque/speed envelope for the benchmark SRM.

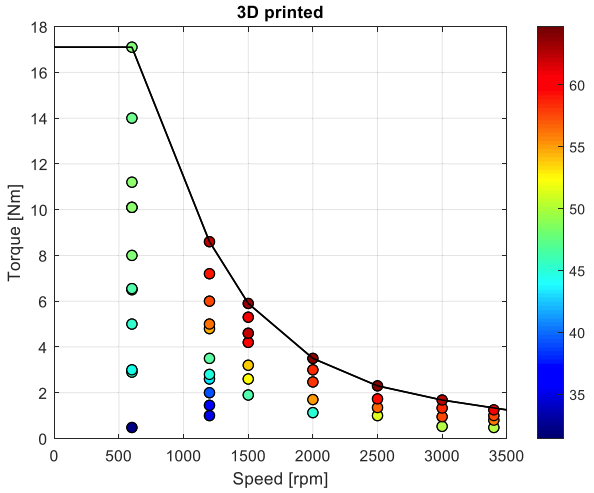

FIGURE 12. Measured efficiency map and torque/speed envelope for the 3DP-SRM.

TABLE 4. Measured quantities at base speed.

Measured quantities	Benchmark SRM	3DP-SRM
Mechanical Power	1170 W	1020 W
Electric Power	1995 W	2130 W
Average phase current	3.27 A	3.31 A
RMS phase current	4.11 A	4.17 A

TABLE 5. Measured quantities at 2.5 times the base speed.

Measured quantities	Benchmark SRM	3DP-SRM
Mechanical Power	960 W	925 W
Electric Power	1149 W	1420 W
Average phase current	1.74 A	1.77 A
RMS phase current	2.13 A	2.44 A

C. TIME DOMAIN ANALYSIS AND DISCUSSION

Comparing the time domain electric quantities for both machines provides a more insightful analysis into the

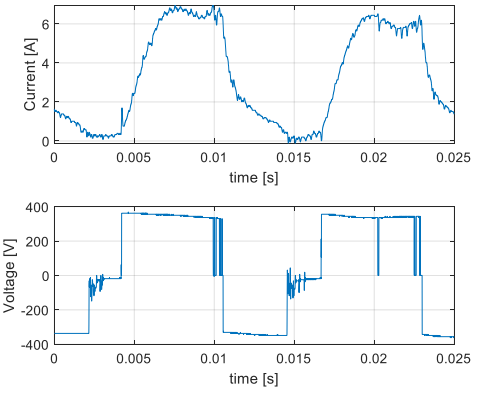

FIGURE 13. Voltage and current for the benchmark SRM at base speed and rated torque.

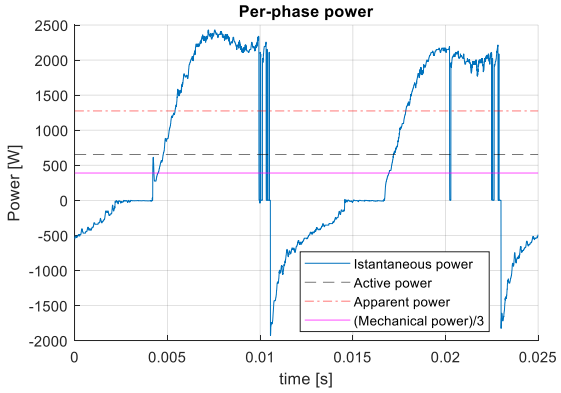

FIGURE 14. Instantaneous power for the benchmark SRM at base speed and rated torque.

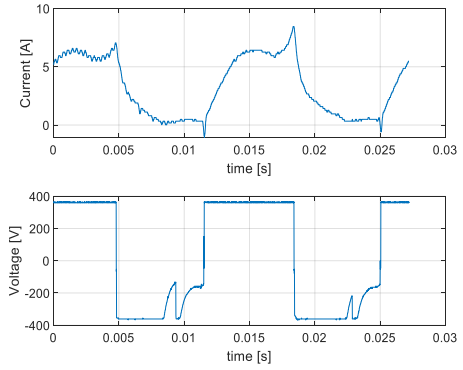

FIGURE 15. Voltage and current for the 3D printed SRM at base speed and rated torque.

experimental results. In particular, in Figure 13 and Figure 14 the instantaneous electric quantities for the benchmark SRM running at base speed are plotted. Similarly, Figures 15 and 16 report the measured electric quantities for the 3DP-SRM operating at 600 rpm.

For the benchmark EM (i.e. Figure 13), it was possible to observe the soft-chopping action, necessary to maintain the current within the hysteresis band. Conversely, a flat-topped voltage waveform was recorded for the 3DP-SRM

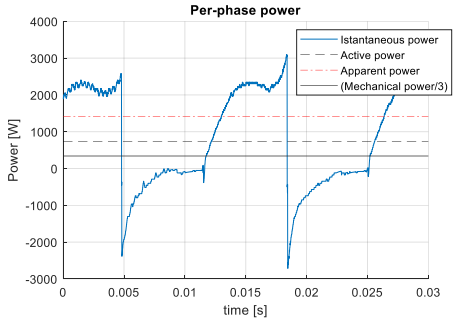

FIGURE 16. **Instantaneous power for the 3DP-SRM at base speed and rated torque.**

(i.e. Figure 15). This indicates that the power electronics converter has actually reached its current limit. Such an observation was also confirmed by the time-period of current / voltage waveforms. Indeed, for the benchmark EM, two electrical periods last 25ms, whilst they last c.a. 27ms for the 3DP-SRM. Accordingly, by calculating the mechanical speed using (2), where f_{el} was the electrical frequency, it was possible to verify that the 3DP-SRM was actually slowing down by c.a. 45 rpm.

$$\omega_m[rpm] = \frac{60 \cdot f_{el}}{Rotor\ Poles} \tag{2}$$

Further considerations can be made by analysis of the instantaneous power waveforms (Figure. 14 and 16). By calculating the ratio between active and apparent power, it was possible to obtain the power factor. At base speed this was equal to 0.52 for both machines. This interesting result indicates that, in principle, the volt-ampere rating of the power converter for a 3DP-SRM can be identical to a standard laminated one (with the same rated power).

However, for the 3DP-SRM in this investigation, because of the increased rotor losses caused by the solid rotor structure, the power converter results are slightly underrated. In fact, the RMS input power for the benchmark SRM was 3.83 kVA, whilst it was equal to 4.24 kVA for the 3DP-SRM. The larger demanded apparent power was needed for partially compensating the efficiency reduction, which can be calculated as the ratio between average mechanical power and average electric power. In particular, the efficiency reduction (at base speed) was c.a. 22 %. As the operating speed was increased, the efficiency of both machines rises accordingly; peaking at c.a. 83 % for the benchmark SRM and 65 % for the 3DP-SRM. Such behaviour was mainly ascribable to the progressively decreasing RMS phase current with increasing speed (for constant and decreasing power operating conditions). Accordingly, the stator Joule losses tend to decrease at high speed, leading to a higher overall efficiency for both machines.

VI. CONCLUSION

Additive manufacturing is considered one of the main enablers for future, high performance electrical machines. This work demonstrates the high technology readiness level of 3D printing and more specifically LPBF, as a manufacturing method for soft magnetic materials employed in electrical machines.

Starting from the raw material (i.e. soft magnetic powder), a complete, test-ready rotor has been manufactured through LPBF and coupled to an existing commercial switched reluctance stator. Comprehensive experimental tests have been carried out, covering the whole torque / speed envelope. The obtained results have been compared to those experimentally recorded on an identical, benchmark machine, featuring a conventional, laminated rotor.

Clearly, because the rotor was a relatively simple solid block with no laminations, its losses were considerably higher with respect to the benchmark machine due to higher eddy current losses. However, in terms of output power and efficiency up to 600rpm (i.e. rated speed) the overall behavior of both SRMs is comparable. Thanks to the strengths of additive manufacturing, a more geometrically complex, magnetically optimized rotor could be easily built for improved overall machine efficiency. Nonetheless, the main objective of this work was achieved. Namely, to prove that additive manufacturing for electric motors is viable and feasible from a manufacturing and technological point of view.

Future work will investigate a multi-objective, 3D finite element optimization and how the magnetic structure can be modified / improved in order to mitigate the effect of eddy current losses. The study highlights comparable behaviour within the low speed region, while improvements to contain the core losses are required at higher speed.

REFERENCES

[1] N. Hopkinson, R. J. M. Hague, and P. M. Dickens, *Rapid Manufacturing*. Chichester, U.K.: Wiley, 2005.

[2] H. Tiismus, A. Kallaste, A. Belahcen, A. Rassolkin, and T. Vaimann, "Challenges of additive manufacturing of electrical machines," in *Proc. IEEE 12th Int. Symp. Diag. Electr. Mach., Power Electron. Drives (SDEMPED)*, Toulouse, France, Aug. 2019, pp. 27–30.

[3] M. Garibaldi, C. Gerada, I. Ashcroft, R. Hague, and H. Morvan, "The impact of additive manufacturing on the development of electrical machines for MEA applications: A feasibility study," in *Proc. 3rd Int. Conf. More Electr. Aircr. (MEA)*, no. 1, 2015, pp. 2–5.

[4] E. Aguilera, J. Ramos, D. Espalin, F. Cedillos, D. Muse, R. Wicker, and E. MacDonald, "3D printing of electro mechanical systems," in *Proc. 24th Solid Freeform Fabr. Symp. (SFF)*, 2013, pp. 950–961.

[5] Z.-Y. Zhang, K. J. Jhong, C.-W. Cheng, P.-W. Huang, M.-C. Tsai, and W.-H. Lee, "Metal 3D printing of synchronous reluctance motor," in *Proc. IEEE Int. Conf. Ind. Technol. (ICIT)*, Mar. 2016, pp. 1125–1128.

[6] S. Lammers, G. Adam, H. J. Schmid, R. Mrozek, R. Oberacker, M. J. Hoffmann, F. Quattrone, and B. Ponick, "Additive manufacturing of a lightweight rotor for a permanent magnet synchronous machine," in *Proc. 6th Int. Electr. Drives Prod. Conf. (EDPC)*, Nov. 2016, pp. 41–45.

[7] R. Wrobel and B. Mecrow, "Additive manufacturing in construction of electrical machines—A review," in *Proc. IEEE Workshop Electr. Mach. Design, Control Diagnosis (WEMDCD)*, Athens, Greece, Apr. 2019, pp. 22–23.

[8] M. Garibaldi, "Can we '3D-Print' an electric motor?" Inst. Aerosp. Technol., Univ. Nottingham, Nottingham, U.K., Aug. 2015. [Online]. Available: https://blogs.nottingham.ac.uk/innovate/2015/08/10/can-we-3d-print-an-electric-motor/

[9] M. Garibaldi, I. Ashcroft, M. Simonelli, and R. Hague, "Metallurgy of high-silicon steel parts produced using selective laser melting," *Acta Mater.*, vol. 110, pp. 207–216, May 2016.

[10] C. Silbernagel, L. Gargalis, I. Ashcroft, R. Hague, M. Galea, and P. Dickens, "Electrical resistivity of pure copper processed by medium-powered laser powder bed fusion additive manufacturing for use in electromagnetic applications," *Additive Manuf.*, vol. 29, Oct. 2019, Art. no. 100831.
[11] C. Silbernagel, I. Ashcroft, P. Dickens, and M. Galea, "Electrical resistivity of additively manufactured AlSi10Mg for use in electric motors," *Additive Manuf.*, vol. 21, pp. 395–403, May 2018.
[12] B. Zhang, N. Fenineche, L. Zhu, H. Liao, and C. Coddet, "Studies of magnetic properties of permalloy (Fe-30% Ni) prepared by SLM technology," *J. Magn. Magn. Mater.*, vol. 324, pp. 495–500, Feb. 2012.
[13] T. Riipinen, S. Metsa-Kortelainen, T. Lindroos, J. S. Keranen, A. Manninen, and J. P. Makelainen, "Properties of soft magnetic Fe-Co-V alloy produced by laser powder bed fusion," *Rapid Prototyping J.*, vol. 25, pp. 699–707, Mar. 2019.
[14] J. N. Lemke, M. Simonelli, M. Garibaldi, I. Ashcroft, R. Hague, M. Vedani, R. Wildman, and C. Tuck, "Calorimetric study and microstructure analysis of the order-disorder phase transformation in silicon steel built by SLM," *J. Alloys Compounds*, vol. 722, pp. 293–301, Mar. 2017.
[15] M. Garibaldi, I. Ashcroft, J. N. Lemke, M. Simonelli, and R. Hague, "Effect of annealing on the microstructure and magnetic properties of soft magnetic Fe-Si produced via laser additive manufacturing," *Scripta Mater.*, vol. 142, pp. 121–125, Jan. 2018.
[16] M. Garibaldi, I. Ashcroft, N. Hillier, S. A. C. Harmon, and R. Hague, "Relationship between laser energy input, microstructures and magnetic properties of selective laser melted Fe-6.9% wt Si soft magnets," *Mater. Characterisation*, vol. 143, pp. 144–151, Sep. 2018.
[17] A. Plotkowski, J. Pries, F. List, P. Nandwana, B. Strump, K. Carver, and R. R. Dehoff, "Influence of scan pattern and geometry on the microstructure and soft-magnetic performance of additively manufactured Fe-Si," *Additive Manuf.*, vol. 29, Oct. 2019, Art. no. 100781.
[18] H. S. Hong, H.-C. Liu, G.-C. Jeong, and J. Lee, "Design of high-end SynRM based on 3D printing technology," in *Proc. IEEE Conf. Electromagn. Field Comput. (CEFC)*, Miami, FL, USA, Nov. 2016, pp. 13–16.
[19] S. Urbanek, B. Ponick, A. Taube, K-P. Hoyer, M. Schaper, S. Lammers, T. Lieneke, and D. Zimmer, "Additive manufacturing of a soft magnetic rotor active part and shaft for a permanent magnet synchronous machine," in *Proc. IEEE Transp. Electrific. Conf. Expo (ITEC)*, Jun. 2018, pp. 217–219.
[20] M. Garibaldi, C. Gerada, I. Ashcroft, and R. Hague, "Free-form design of electrical machine rotor cores for production using additive manufacturing," *J. Mech. Des.*, vol. 141, no. 7, pp. 071401-1–071401-13, Jul. 2019, doi: 10.1115/1.4042621.
[21] A. Hughes, *Electric Motors and Drives: Fundamentals, Types and Applications*, 4th ed. Oxford, U.K.: Newnes, 2013.
[22] D.-H. Lee, T. Hieu Pham, and J.-W. Ahn, "Design and operation characteristics of four-two pole high-speed SRM for torque ripple reduction," *IEEE Trans. Ind. Electron.*, vol. 60, no. 9, pp. 3637–3643, Sep. 2013.
[23] H. Zhang, W. Xu, S. Wang, Y. Huangfu, G. Wang, and J. Zhu, "Optimum design of rotor for high-speed switched reluctance motor using level set method," *IEEE Trans. Magn.*, vol. 50, no. 2, pp. 765–768, Feb. 2014.
[24] M. Littmann, "Iron and silicon-iron alloys," *IEEE Trans. Magn.*, vol. MAG-7, no. 1, pp. 48–60, Mar. 1971.
[25] R. S. Sundar and S. C. Deevi, "Soft magnetic FeCo alloys: Alloy development, processing, and properties," *Int. Mater. Rev.*, vol. 50, no. 3, pp. 157–192, 2005.
[26] S. Tumanski, *Handbook of Magnetic Measurements*. Boca Raton, FL, USA: CRC Press, 2011.
[27] A. J. Moses, "Electrical steels: Past, present and future developments," *IEE Proc. A, Phys. Sci., Meas. Instrum., Manage. Edu.*, vol. 137, no. 5, pp. 233–245, Sep. 1990.
[28] T. Ferreira and W. Rasband, "ImageJ user guide," *ImageJ/Fiji*, vol. 1, pp. 155–161, May 2012.
[29] *E8/E8M-13a.(2013).'Standard Test Methods for Tension Testing of Metallic Materials'*, ASTM Int., West Conshohocken, PA, USA, 2013.
[30] *E92-16 Standard Test Methods for Vickers Hardness and Knoop Hardness of Metallic Materials*, ASTM Int., West Conshohocken, PA, USA, 2016.
[31] *B193-02 Standard Test Method for Resistivity of Electrical Conductor Materials*, ASTM Int., West Conshohocken, PA, USA, 2014.

LEONIDAS GARGALIS is currently pursuing the Ph.D. degree. He is also a Research Assistant with the Centre for Additive Manufacturing (CfAM). After, he received a Marie Curie Doctoral Fellowship in 2016, he joined CfAM and the Institute for Aerospace Technology at the University of Nottingham. His research has focused on developing soft magnetic alloys using selective laser melting for the design and fabrication of rotating electrical machines. His research interests include metal AM span between process optimization, such as parametric studies for materials qualification, and characterization of 3D printed materials such as the microstructural, mechanical, and electromagnetic properties.

VINCENZO MADONNA (Member, IEEE) received the M.Sc. degree in electrical engineering from the University of Bologna, Italy, in 2016, and the Ph.D. degree in electrical machines design from the University of Nottingham, U.K., in 2020. In 2016, he was awarded a prestigious Marie Curie Doctoral Fellowship and joined the Institute for Aerospace Technology in Nottingham. He is currently a Research Fellow with the Propulsion Futures Beacon of Excellence, University of Nottingham. His research interests include design, thermal management, and lifetime prediction modeling of electrical machines.

PAOLO GIANGRANDE (Senior Member, IEEE) received the Ph.D. degree in electrical engineering from the Politecnico of Bari, in 2011. Since 2012, he has been a Research Fellow with the Power Electronics, Machines, and Control (PEMC) Group, University of Nottingham, U.K. In 2019, he was appointed as a Senior Research Fellow with the PEMC Group, where he is also the Head of the Accelerated Lifetime Testing Laboratory. His main research interests include design and testing of electromechanical actuators for aerospace, thermal management of high-performance electric drives, and reliability of electrical machines.

ROBERTO ROCCA (Member, IEEE) was born in Rome, in 1989. He received the M.S. degree (Hons.) in electrical engineering from the Sapienza University of Rome, Rome, Italy, in 2015, and the Ph.D. degree in electrical and electronics engineering from the Power Electronics, Machines, and Control (PEMC) Group, University of Nottingham, Nottingham, U.K., in 2020. From 2019 to 2020, he served as a Research Associate for the Department of Astronautical, Electrical, and Energy Engineering (DIAEE), Sapienza University of Rome. He is currently serving as a Research Assistant for Fundación Research Centre for Energy Resources and Consumption (CIRCE), Zaragoza, Spain, in the research area of analysis, operation, and control of electrical grids with high-penetration of renewable energy sources.

MARK HARDY is currently a Senior Research Technician with the Centre for Additive Manufacture, University of Nottingham, U.K. He has been working in the AM field for the past ten years and has a background of more than 20 year's Mechanical Engineering experience in the Power Generation sector. His main focus is on Selective Laser Melting with interests in all aspects of Additive Manufacturing.

IAN ASHCROFT is currently a Professor of Solid Mechanics, a member of the Centre for Additive Manufacturing (CfAM), and the Head of the Department-Mechanical, Materials, and Manufacturing, Faculty of Engineering, University of Nottingham. His areas of knowledge encompass static and dynamic loading, design optimization, heat, and mass transport and material microstructure understanding. His current research interests include materials testing and characterization, multi-physics finite element analysis, design for manufacture, and structural and multi-objective optimization.

MICHAEL GALEA (Senior Member, IEEE) received the Ph.D. degree in electrical machines design from the University of Nottingham, Ningbo, China. He has worked as a Research Fellow with the University of Nottingham, where he is currently the Head of the School of Aerospace, and a Professor in Electrical Machines and Drives. His main research interests include design, analysis and thermal management of electrical machines and drives, and the more electric aircraft and electrified and hybrid propulsion.

RICHARD HAGUE is currently a Professor of Innovative Manufacturing with the Department of Mechanical, Materials, and Manufacturing Engineering, University of Nottingham, the Head of the Centre for Additive Manufacturing (CfAM), and the Director of the EPSRC Centre for Innovative Manufacturing in Additive Manufacturing. He has been working in the AM field for 20 years and has a background of leading and managing large multi-disciplinary and multi-partner research projects. His research interests include AM specific processes, materials and design / design systems across a wide spectrum of industrial sectors with a particular interest in design / design systems.